Graphical Abstract

Delamination growth of a sandwich layer by diffusion of a corrosive species

Alessandro Leronni, Norman A. Fleck

Delamination of an adhesive sandwich layer by diffusion of a corrodent

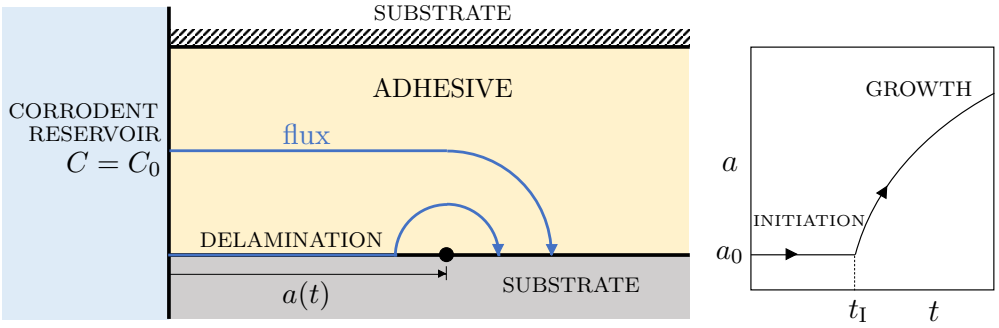

Highlights

Delamination growth of a sandwich layer by diffusion of a corrosive species

Alessandro Leronni, Norman A. Fleck

- Prediction of growth rate for delamination of a sandwich layer by corrodent diffusion
- Map displays regimes of behaviour with contours of delamination growth rate
- Singularity analysis at the delamination tip for slow delamination of a thick layer

Delamination growth of a sandwich layer by diffusion of a corrosive species

Alessandro Leronni, Norman A. Fleck*

Cambridge University Engineering Department, Trumpington Street, Cambridge, CB2 1PZ, UK

Abstract

The progressive delamination of a sandwich layer is analysed by assuming that delamination is driven by Fickian diffusion of a corrosive species. One side face of the layer is exposed to a constant concentration of corrodent and the corrodent diffuses along both the sandwich layer and the delamination. The corrodent is consumed ahead of the delamination tip by a first-order chemical reaction on the interface; when a critical amount of corrodent has reacted, the delamination front advances, thereby setting the delamination growth criterion. Numerical solutions are obtained for growth of the delamination as a function of time over the full range of geometric and material parameters. Analytic solutions are obtained for asymptotic regimes of behaviour, with an emphasis on the case of slow growth subsequent to an initiation period.

Keywords:

adhesion and adhesives, corrosion and embrittlement, delamination, diffusion, fracture

*Corresponding author

Email addresses: al2040@cam.ac.uk (Alessandro Leronni), naf1@cam.ac.uk (Norman A. Fleck)

1. Introduction

Multi-layers are increasingly used in engineering design, for example adhesive joints in the form of a thin layer sandwiched between two stiff substrates (**????**). The structural integrity of the sandwich layer is a concern, particularly in the presence of a corrosive environment (**???**). A prototypical practical example is an adhesive layer sandwiched between a steel substrate and a composite superstructure in primary ship structures (**?**). Compared to traditional steel solutions with bolted or welded connections, adhesively-bonded hybrid structures offer a number of advantages, including reductions in weight, in fuel consumption and in harmful emissions. However, both the commercialisation and qualification of these joints are hampered by a limited knowledge of their long-term behaviour.

An experimental literature exists on the degradation of an adhesive joint by ageing mechanisms that involve diffusion of a corrosive species. Commonly, chemical ageing gives rise to a degradation of modulus and strength of the bulk adhesive, and may also result in swelling (**???**). Although moisture and contamination degrade the adhesive, the failure of a bonded joint due to environmental attack is ultimately interfacial in nature (**???**). A number of complex chemical reactions lead to ageing of the interface between adhesive and substrate. For example, the hydrolysis of interfacial covalent bonds between adhesive and metal oxide can occur in the presence of moisture; hydration can also weaken a metal oxide layer (**?**). Some authors replace the interface by an interphase of small but finite thickness, with different mechanical and diffusion properties than those of the bulk (**???**). A phase field approach can also be adopted to model an interphase of boundary layer

thickness that ages (**??**).

It has recently been shown that steel/adhesive/steel sandwich specimens, representative of large-scale ship joints, may undergo progressive delamination when immersed in oxygenated salt water (**?**). The present study, motivated by the experiments of **?**, contains an analysis of the general problem of a corrodent that diffuses down its concentration gradient along two competing paths, a bulk path (the adhesive) and a surface path (the delaminated interface between adhesive and substrate). The corrodent reacts with the intact adhesive/substrate interface immediately ahead of the crack tip, eventually leading to delamination growth.

A practical example is the diffusion of moisture (water vapour) in an adhesive layer and along the delamination, with attack occurring on the intact interface (**????**). In this case, the usual assumption is that a water-saturated thin layer of adhesive is instantaneously established on the adhesive surface in contact with water. This layer acts as a water reservoir with constant concentration, corresponding to the solubility limit of water in the adhesive. This is typically equal to a few percentage points weight by weight and varies with environmental conditions (**?**; **?**, Section B.4). Fickian diffusion is commonly assumed as a phenomenological law for moisture diffusion in adhesives (**?**). However, more complex diffusion models have been proposed, such as the Langmuir model (**?**) and the dual Fickian model (**?**). Typically, Fick's law ceases to be valid at high temperatures. The overall effective value of diffusion coefficient of joint material exceeds that of the bulk adhesive (**?**). To explain this, many authors account for fast diffusion along the adhesive/substrate interface (**??**). **?** explain that the presence of a surface

treatment controls interfacial diffusion. For example stainless steel, after sandblasting, has a reactive surface that is instantaneously covered by oxides; secondary interfacial bonds are present and these are rapidly weakened in contact with moisture, thereby allowing for rapid diffusion along the degraded interface. The same type of problems can arise in fibre-reinforced composites, where water diffusion along the interface between matrix and fibres can lead to delamination, see for example **?**. Note that the concentration-driven diffusion of moisture differs from hydraulic fracture wherein a fluid is driven along a crack by a pressure gradient. Hydraulic fracture pertains to the case where pressurised fluid is pumped into a crack and leaks into the porous medium adjacent to the crack flanks (**??**). Finally, to describe dissociation of bonds between polymers and metals by interfacial hydrolysis, a first-order irreversible reaction can be considered (**?**).

The phenomenon of cathodic delamination of a thin adhesive coating in the presence of salt water is well-established (**??**). When the concentration of dissolved oxygen at the crack tip is sufficiently high, the rate-limiting step for delamination is the diffusion of cations, such as sodium ions, to the crack tip. In contrast, when the oxygen concentration is low, as for the case of an adhesive sandwich layer, the rate controlling step becomes that of oxygen diffusion along the delamination and in the adhesive (**?**). Thus, the model introduced in the present study has also direct relevance to oxygen-limiting cathodic delamination.

As a final example, our model can be used to describe the diffusion of chloride ions into unsaturated concrete from the outside environment. When a sufficient amount of free chlorides dissolved in the pore solution of the

concrete reaches a reinforcing bar, the oxide passive layer is attacked and the corrosion process is initiated (**?**, Chapter 2).

The overall aim of the present study is to give a simple but versatile framework to study the progressive debonding of an adhesive joint when the migration of a single corrosive species is governed by diffusion. The full time-dependent problem is solved numerically. Regimes of behaviour are identified and discussed, and analytical solutions are given to quantify the expected growth rate of the delamination.

This work complements the study of **?**: they calculated the incubation time to initiate delamination advance from a pre-existing defect. Attention is focused on the case where the critical amount of corrodent for debonding is sufficiently large to ensure that the delamination growth rate is slow, to be made precise below. In this regime, the asymptotic solutions of **?** for the initiation problem are extended to obtain the subsequent growth rate of the delamination. The case of fast growth is also considered, and the steady-state limit of **?** is retrieved for the case where surface diffusion along the delamination dominates over bulk diffusion in the adhesive. Our study is of broad relevance to the life prediction of engineering structures due to corrosion. Corrosion remains a ubiquitous and expensive challenge to the engineering industry and there is a clear need for the development of lifing methodologies that include both initiation and growth.

The study is organised as follows. The formulation of the time-dependent delamination growth problem is presented in Section 2. The numerical solution is given and regimes of behaviour are identified for a thick and for a thin sandwich layer in Sections 3 and 4, respectively. The transition

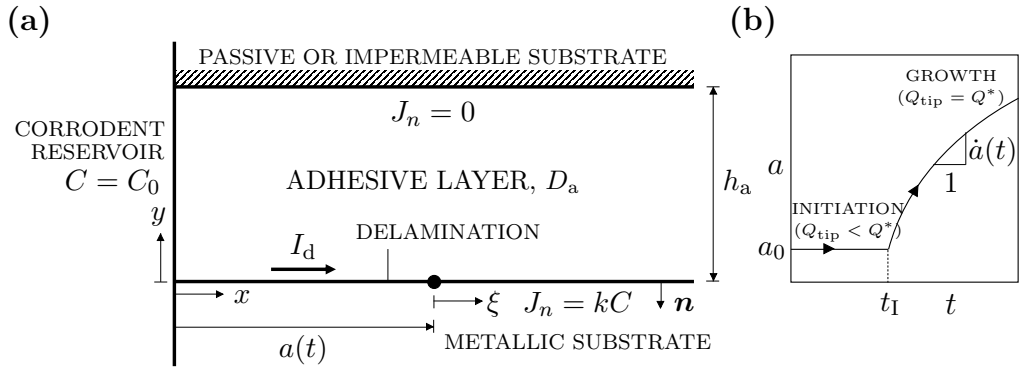

Figure 1: Delamination of an adhesive sandwich layer by diffusion of a corrosive species: **(a)** sketch of the problem and **(b)** qualitative solution in terms of delamination length against time.

of response between thick and thin adhesive layer is discussed in Section 5, and the sensitivity of delamination rate to initial delamination length is addressed in Section 6, before drawing conclusions in Section 7. The numerical implementation of the governing equations is detailed in Appendix A.

2. Time-dependent delamination growth

With reference to Fig. 1, consider an adhesive sandwich layer of height h_a and semi-infinite length, with a face on $x = 0$. The lower interface of the layer contains a delamination of length $a(t)$ at a representative time t. The concentration of corrodent within the adhesive layer is $C(x, y, t)$, and vanishes initially (at $t = 0$). Assume that the delamination length $a(t)$ has an initial value of $a(0) = a_0$.

Corrodent is supplied from the left-side face of the adhesive, which is maintained at a fixed concentration $C = C_0$ by a corrodent reservoir such

that

$$C = C_0\,, \qquad x = 0,\, 0 < y < h_{\mathrm{a}} \tag{1}$$

Assume that Fickian diffusion occurs within the adhesive layer and within the delamination. Denote the diffusion coefficient of corrodent in the adhesive by D_{a}. Then, the corrodent flux in the layer is given by $\boldsymbol{J} = -D_{\mathrm{a}}\boldsymbol{\nabla} C$, where $\boldsymbol{\nabla}$ is the usual gradient operator. Mass conservation of the corrodent implies

$$\frac{\partial C}{\partial t} + \boldsymbol{\nabla}\cdot\boldsymbol{J} = 0 \tag{2}$$

where $\boldsymbol{\nabla}\cdot$ is the usual divergence operator. Upon making use of mass conservation (2) and Fick's law, the governing diffusion equation in the adhesive reads

$$\frac{\partial C}{\partial t} = D_{\mathrm{a}}\left(\frac{\partial^2 C}{\partial x^2} + \frac{\partial^2 C}{\partial y^2}\right) \tag{3}$$

The delaminated interface acts as an additional path for surface diffusion of the corrodent. Specifically, as shown in Fig. 1, the delaminated interface carries a current I_{d} of corrodent given by

$$I_{\mathrm{d}} = -K_{\mathrm{d}}\frac{\partial C}{\partial x}\,, \qquad 0 < x < a(t),\, y = 0 \tag{4}$$

where the parameter K_{d}, with units of m^3/s, controls the rate of surface diffusion. Mass conservation implies that $J_n = \partial I_{\mathrm{d}}/\partial x$, such that the following boundary condition holds along the delaminated interface:

$$J_n = -K_{\mathrm{d}}\frac{\partial^2 C}{\partial x^2}\,, \qquad 0 < x < a(t),\, y = 0 \tag{5}$$

The additional condition $\partial C/\partial x = 0$ at $x = a^-(t), y = 0$ is prescribed to ensure that a point source of corrodent does not exist at the delamination tip.

The consumption of corrodent along the pristine adhesive/metal interface is dictated by a first-order chemical reaction with rate constant k:

$$J_n = kC\,, \qquad x > a(t),\, y = 0 \tag{6}$$

and a material length scale $l \equiv D_\mathrm{a}/k$ emerges immediately.

Finally, take the upper boundary of the adhesive layer at $y = h_\mathrm{a}$ as insulating, such that $J_n = 0$. This may indicate that the top substrate is in a passivated state or is impermeable, as shown in Fig. 1. Alternatively, this boundary may be regarded as a plane of symmetry for a metal/adhesive/metal sandwich with adhesive layer of height $2h_\mathrm{a}$.

The total amount of corrodent per unit area Q that has reacted at time t on the adhesive/metal interface is given by

$$Q(x,t) = \int_0^t J_n(x, y=0, t')\,\mathrm{d}t'\,, \qquad x > a(t) \tag{7}$$

Define Q directly ahead of the delamination tip as $Q_\mathrm{tip}(t) \equiv Q(a^+(t), t)$. As shown in Fig. 1(b), the delamination of initial length a_0 starts to advance after an initiation time t_I, such that Q_tip attains a critical value Q^*. Subsequently, the delamination propagates at a rate $\dot{a}(t) \equiv \mathrm{d}a/\mathrm{d}t$, in accordance with the growth criterion

$$Q_\mathrm{tip}(t \geq t_\mathrm{I}) = Q^* \tag{8}$$

It remains to solve the coupled problem for the concentration $C(x, y, t)$ in the adhesive layer and for the delamination length $a(t)$. The commercial finite element software *COMSOL Multiphysics*, version 5.6, is used to obtain $C(x, y, t)$ and $a(t)$. The details are given in Appendix A. The solution can be expressed in non-dimensional form as follows:

$$\frac{C}{C_0} = f_1\left(\frac{x}{l}, \frac{y}{l}, \frac{D_\mathrm{a}t}{l^2}; \frac{h_\mathrm{a}}{l}, \frac{K_\mathrm{d}}{lD_\mathrm{a}}, \frac{Q^*}{C_0 l}\right) \tag{9a}$$

and

$$\frac{a}{l} = f_2\left(\frac{D_\mathrm{a}t}{l^2}; \frac{h_\mathrm{a}}{l}, \frac{K_\mathrm{d}}{lD_\mathrm{a}}, \frac{Q^*}{C_0 l}\right) \tag{9b}$$

in terms of the two functions f_1 and f_2.

3. Numerical solution and regimes of behaviour for a thick sandwich layer

Numerical solutions are first obtained for a large adhesive height such that $h_\mathrm{a}/l = 1000$, and in the absence of an initial pre-crack, $a_0 = 0$. The time-dependent problem is solved for several combinations of $K_\mathrm{d}/(lD_\mathrm{a})$ and $Q^*/(C_0 l)$. The delamination length is obtained as a function of time; then, numerical differentiation provides the growth rate $\dot{a}$. A contour map of $\dot{a}/k$ as a function of $K_\mathrm{d}/(lD_\mathrm{a})$ and $Q^*/(C_0 l)$ for the choice $a/l = 100$ is given in Fig. 2(a).[1] Four representative cases, corresponding to four asymptotic regimes of delamination response, are denoted on this map by the discrete data points A, B, C and D. For each of these cases, the interfacial flux ahead of the delamination tip is given in Fig. 2(b) for the choice $a/l = 100$; curves for a/l as a function of $D_\mathrm{a}t/l^2$, and $\dot{a}/k$ as a function of a/l, are given in Fig. 2(c) and (d), respectively. Note that delamination growth begins after an initiation time $t_\mathrm{I} = Q^*/(kC_0)$, see Fig. 2(c). The four regimes of behaviour are now

[1] Given the smooth *COMSOL* solution for $a(t)$, the growth rate $\dot{a}(t)$ is obtained through numerical differentiation in *MATLAB* via the function `gradient`. This procedure may lead to numerical oscillations, which are mitigated via the function `smooth`. The contour map of Fig. 2(a) is also obtained in *MATLAB* by using 49 combinations of $K_\mathrm{d}/(lD_\mathrm{a})$ and $Q^*/(C_0 l)$ values, with additional simulations at salient points to confirm that the contour map is accurate in the region where the contour spacing changes in a significant way.

described, followed by an analytical treatment of each. For compactness of notation, the same labelling is used for representative cases as for regimes.

Regime A: *Error function regime*

In this regime, bulk diffusion in the adhesive is dominant, $K_\mathrm{d}/(lD_\mathrm{a}) \ll 1$, and $Q^*/(C_0 l)$ is sufficiently small for delamination growth to be fast, $\dot{a}/k \gg 1$. The concentration profile is one-dimensional along x and is adequately described by the error function solution (**?**). Consequently, the delamination length is approximately proportional to the square root of time.

Regime B: *Boundary layer regime*

Surface diffusion along the delamination is dominant, $K_\mathrm{d}/(lD_\mathrm{a}) \gg 1$, and $Q^*/(C_0 l)$ is again sufficiently small for delamination growth to be fast, $\dot{a}/k \gg 1$. A constant growth rate is established and the concentration decays from C_0 to zero in a small boundary layer ahead of the delamination tip, as derived by **?**.

Regime C: *K-field regime*

Bulk diffusion in the adhesive is dominant, $K_\mathrm{d}/(lD_\mathrm{a}) \ll 1$, and $Q^*/(C_0 l)$ is sufficiently large for delamination growth to be slow, $\dot{a}/k \ll 1$. For $a/l \gg 1$, the flux more than a distance l ahead of the delamination tip is characterised by an inverse square root singularity reminiscent of the K-field in fracture mechanics (**?**). The growth rate $\dot{a}$ is constant provided $a/h_\mathrm{a} \ll 1$.

Regime D: *Dislocation field regime*

Surface diffusion along the delamination is dominant, $K_\mathrm{d}/(lD_\mathrm{a}) \gg 1$, and $Q^*/(C_0 l)$ is sufficiently large for delamination growth to be slow, $\dot{a}/k \ll 1$. For $a/l \gg 1$, the flux more than a distance l ahead of the delamination tip is

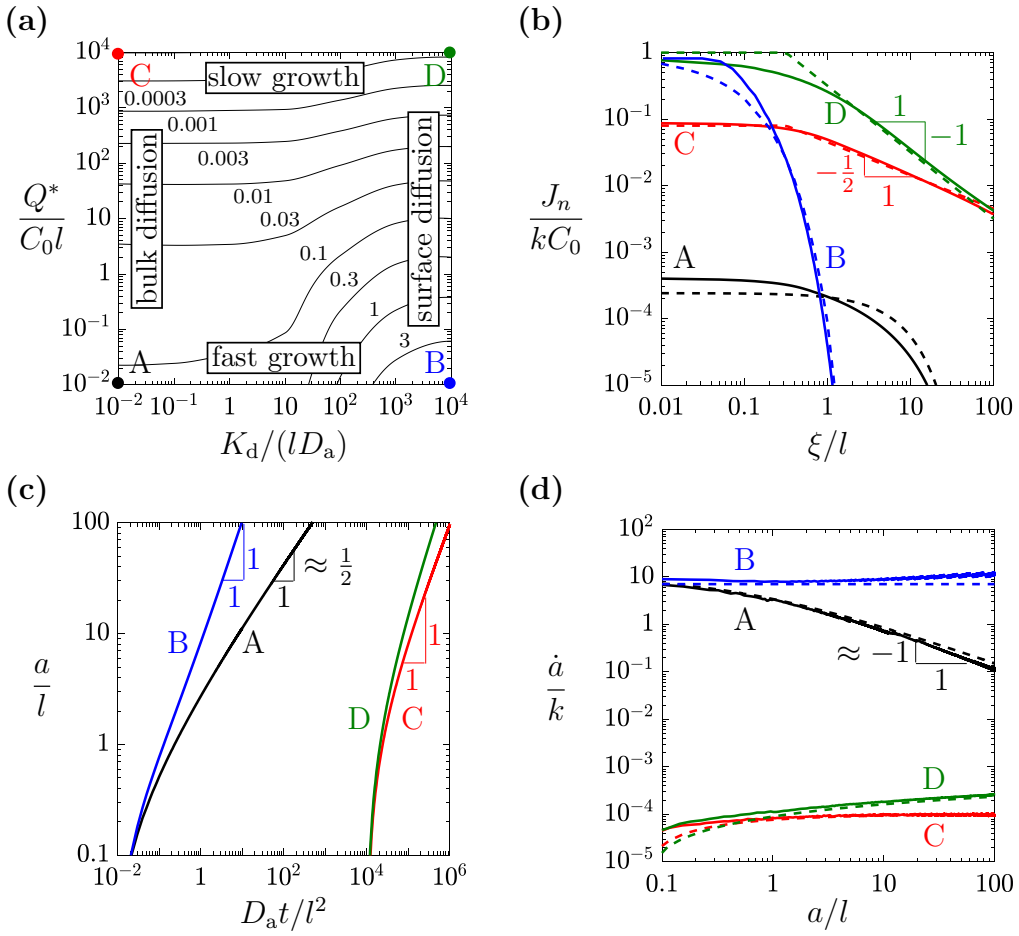

Figure 2: A thick sandwich layer. Solid lines and dashed lines refer to numerical solutions of the full time-dependent problem for $a_0 = 0$ and $h_\mathrm{a}/l = 1000$ (see Section 2) and to analytic solutions (as given in Sections 3.1-3.6), respectively. Regimes A, B, C and D correspond to the error function, boundary layer, K-field and dislocation field regimes, respectively. **(a)** contours of $\dot{a}/k$ on a plot with axes $K_\mathrm{d}/(lD_\mathrm{a})$ and $Q^*/(C_0 l)$ for the choice $a/l = 100$; **(b)** interfacial flux ahead of the delamination tip for $a/l = 100$; **(c)** delamination length as a function of time; **(d)** delamination velocity as a function of delamination length.

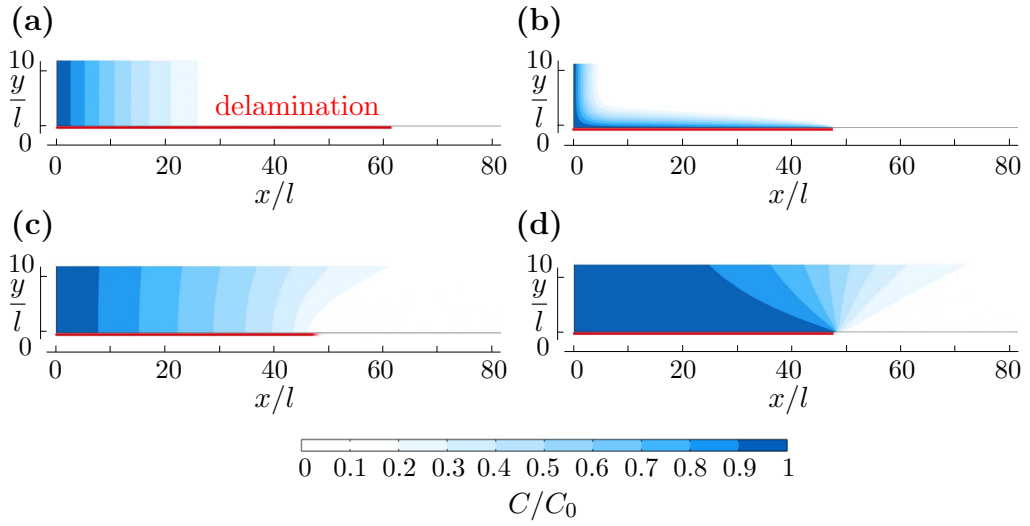

Figure 3: Numerical solution of the full time-dependent problem of Section 2 for a thick sandwich layer, with $a_0 = 0$ and $h_a/l = 1000$. Regimes A, B, C and D are identified in Fig. 2(a). Concentration field in the sandwich layer and delamination length (denoted by a solid red line) at selected times, for regimes **(a)** A (error function regime) at $D_a t/l^2 = 200$, **(b)** B (boundary layer regime) at $D_a t/l^2 = 5$, **(c)** C (K-field regime) at $D_a t/l^2 = 5 \times 10^5$ and **(d)** D (dislocation field regime) at $D_a t/l^2 = 2.5 \times 10^5$.

characterised by an inverse singularity reminiscent of a dislocation field (**?**). The growth rate increases slightly with increasing delamination length, for $a/h_a \ll 1$.

The concentration field $C(x, y)$ and the corresponding delamination length
195 at selected times for regimes A, B, C and D are represented in Fig. 3. Videos for the time evolution of the concentration field and delamination length are provided in the online Supplementary Material.

3.1. Regime A. Fast growth and bulk diffusion: error function regime

Consider the case of fast growth and bulk diffusion, that is, regime A of Fig. 2(a). The numerical solution of Fig. 3(a) suggests that the concentration field is almost one-dimensional along x, and $C(x, y, t)$ can be adequately approximated by $C(x, t)$ using the following analytical treatment. Take $K_\mathrm{d} = 0$ and reduce the 2D time-dependent problem of Section 2 to the following 1D problem:

$$\frac{\partial C}{\partial t} = D_\mathrm{a} \frac{\partial^2 C}{\partial x^2}\,, \qquad 0 < x < a(t) \tag{10a}$$

$$\frac{\partial C}{\partial t} = D_\mathrm{a} \frac{\partial^2 C}{\partial x^2} - \frac{k}{h_\mathrm{a}} C\,, \qquad x > a(t) \tag{10b}$$

with $C = C_0$ at $x = 0$. After introducing the non-dimensional variables $\bar{x} = x/l$ and $\bar{t} = D_\mathrm{a} t/l^2$, equations (10) become

$$\frac{\partial C}{\partial \bar{t}} = \frac{\partial^2 C}{\partial \bar{x}^2}\,, \qquad 0 < \bar{x} < a(\bar{t})/l \tag{11a}$$

$$\frac{\partial C}{\partial \bar{t}} = \frac{\partial^2 C}{\partial \bar{x}^2} - \frac{l}{h_\mathrm{a}} C\,, \qquad \bar{x} > a(\bar{t})/l \tag{11b}$$

In the asymptotic limit $l/h_\mathrm{a} \to 0$, the above 1D problem reduces to solving the equation $\partial C/\partial t = D_\mathrm{a}(\partial^2 C/\partial x^2)$ over $x > 0$, with $C = C_0$ at $x = 0$. The solution is (**?**)

$$C(x, t) = C_0 \,\mathrm{erfc}\left(\frac{x}{2\sqrt{D_\mathrm{a} t}}\right) \tag{12}$$

The interfacial flux ahead of the delamination tip is $J_n = kC$, as demanded by equation (6). The analytical expression for J_n is plotted in Fig. 2(b). Good agreement exists with the full numerical solution. Note that the analytic solution (12) is independent of the value of Q^*.

Now invoke the growth criterion $Q^* = k\int_0^t C(x=a(t),t')\,\mathrm{d}t'$ (resulting from (6), (7) and (8)) to obtain

$$\frac{Q^*}{kC_0t} = \left(\frac{a^2}{2D_\mathrm{a}t}+1\right)\operatorname{erfc}\left(\frac{a}{2\sqrt{D_\mathrm{a}t}}\right) - \frac{a}{\sqrt{\pi D_\mathrm{a}t}}\exp\left(-\frac{a^2}{4D_\mathrm{a}t}\right) \tag{13}$$

In order to compare the analytical prediction (13) with the full numerical prediction of a/l as a function of $D_\mathrm{a}t/l^2$ for a given value of $Q^*/(C_0l)$, it is convenient to first re-express (13) in the form:

$$\frac{Q^*}{C_0l}\frac{l^2}{D_\mathrm{a}t} = \left[\left(\frac{a}{l}\right)^2\frac{l^2}{2D_\mathrm{a}t}+1\right]\operatorname{erfc}\left(\frac{a}{l}\frac{l}{2\sqrt{D_\mathrm{a}t}}\right) - \frac{a}{l}\frac{l}{\sqrt{\pi D_\mathrm{a}t}}\exp\left[-\left(\frac{a}{l}\right)^2\frac{l^2}{4D_\mathrm{a}t}\right] \tag{14}$$

Equation (14) is solved numerically[2] for the delamination length a/l as a function of time $D_\mathrm{a}t/l^2$, with the choice $Q^*/(C_0l) = 0.01$. Then, numerical differentiation provides $\dot{a}/k$. Excellent agreement exists between this solution and the solution of the full time-dependent problem, see Fig. 2(d).

3.2. Quasi-steady delamination growth

In order to discuss regimes of behaviour B, C and D, it is convenient to introduce the moving coordinate ξ with origin at the current delamination tip, such that $\xi(x,t) = x - a(t)$, as shown in Fig. 1. Consequently, $C(x,y,t)$ can be re-phrased as $C(\xi,y,t)$. The governing PDE (3) in (x,y,t) can be re-written in terms of (ξ,y,t) as

$$-\dot{a}(t)\frac{\partial C}{\partial \xi} + \frac{\partial C}{\partial t} = D_\mathrm{a}\left(\frac{\partial^2 C}{\partial \xi^2}+\frac{\partial^2 C}{\partial y^2}\right) \tag{15}$$

Assume that, after an initial transient of growth, a regime of *quasi-steady growth* is attained such that the term $\partial C/\partial t$ is negligible in (15) and the

[2]The `fsolve` function of *MATLAB* is used.

parabolic PDE (15) simplifies to the elliptic PDE

$$\dot{a}\frac{\partial C}{\partial \xi} + D_{\mathrm{a}}\left(\frac{\partial^2 C}{\partial \xi^2} + \frac{\partial^2 C}{\partial y^2}\right) = 0 \tag{16}$$

The boundary conditions (1), (5) and (6) in (x, y) can be re-phrased in terms of (ξ, y) to read

$$C = C_0\,, \qquad \xi = -a, 0 < y < h_{\mathrm{a}} \tag{17a}$$

$$J_n = -K_{\mathrm{d}}\frac{\partial^2 C}{\partial \xi^2}\,, \qquad -a < \xi < 0,\ y = 0 \tag{17b}$$

$$J_n = kC\,, \qquad \xi > 0,\ y = 0 \tag{17c}$$

Note that the solution of (16)-(17) provides $C(\xi, y)$ for any given values of a and $\dot{a}$.

Equations (7) and (8) can be used to obtain a relation for Q^* in the regime of quasi-steady growth, as follows. Note from (7) that

$$\frac{\partial Q(x,t)}{\partial t} = J_n(x, y = 0, t)\,, \qquad x > a(t) \tag{18}$$

and rewrite $Q(x, t)$ as $Q(\xi, t)$ such that (18) can be re-phrased in terms of (ξ, t) to read

$$-\dot{a}(t)\frac{\partial Q(\xi,t)}{\partial \xi} + \frac{\partial Q(\xi,t)}{\partial t} = J_n(\xi, y = 0, t)\,, \qquad \xi > 0 \tag{19}$$

When quasi-steady growth prevails, $\partial Q/\partial t \approx 0$ and (19) reduces to

$$-\dot{a}\frac{\partial Q(\xi)}{\partial \xi} = J_n(\xi, y = 0)\,, \qquad \xi > 0 \tag{20}$$

Finally, integrate both sides of (20) in ξ from $\xi = 0^+$ to $\xi \to \infty$, with $Q(\xi = 0^+) = Q^*$ (as given by (8)) and $\lim_{\xi\to\infty} Q(\xi) = 0$, to obtain

$$Q^* = \frac{1}{\dot{a}}\int_{0^+}^{\infty} J_n(\xi, y = 0)\,\mathrm{d}\xi \tag{21}$$

For any prescribed values of a and $\dot{a}$, $J_n(\xi, y = 0)$ is given by the solution to (16)-(17), and in turn, Q^* is obtained from (21).

The problem defined by (16), (17) and (21) is referred to as the quasi-steady growth problem. Its non-dimensional solution reads

$$\frac{C}{C_0} = f_1\left(\frac{\xi}{l}, \frac{y}{l}; \frac{a}{l}, \frac{h_\mathrm{a}}{l}, \frac{K_\mathrm{d}}{lD_\mathrm{a}}, \frac{\dot{a}}{k}\right) \tag{22a}$$

and

$$\frac{Q^*}{C_0 l} = f_2\left(\frac{a}{l}, \frac{h_\mathrm{a}}{l}, \frac{K_\mathrm{d}}{lD_\mathrm{a}}, \frac{\dot{a}}{k}\right) \tag{22b}$$

Note that time enters the quasi-steady growth problem only implicitly via $\dot{a}$. Therefore, in order to solve the governing equations, it is convenient to assume values for a and $\dot{a}$ and then solve for Q^*.

3.3. Regime B. Fast growth and surface diffusion: boundary layer regime

Consider the case of fast growth under surface diffusion control, that is, regime B of Fig. 2(a). Figure 2(d) suggests that a steady state with constant growth rate is rapidly established, such that the time-independent problem of Section 3.2 applies. Assume that diffusion along the delamination is instantaneous, $K_\mathrm{d} \to \infty$, and that the crack is semi-infinite in extent, $a \to \infty$. Boundary condition (17b) reduces to $C = C_0$ for $\xi < 0$, $y = 0$. **?** have solved this problem by transforming the PDE (16) into an ODE through the Fourier transform and then by using the Wiener–Hopf technique to solve the ODE. The concentration field reads

$$C(\xi, y) = C_0 - \frac{C_0}{\pi} \exp\left(\frac{2k}{\pi\dot{a}}\right) \int_0^\infty \frac{\exp(\rho\dot{a}\xi/D_\mathrm{a})}{\rho\sqrt{1+\rho}} \left(\frac{\sqrt{1+\rho}-\sqrt{\rho}}{\sqrt{1+\rho}+\sqrt{\rho}}\right)^{\frac{k/\dot{a}}{\pi\sqrt{\rho(1+\rho)}}} \times \sin\left[\sqrt{\rho(1+\rho)}\dot{a}y/D_\mathrm{a}\right] \mathrm{d}\rho\,, \qquad \xi < 0\,,\ y > 0 \tag{23a}$$

$$C(\xi,y)=\frac{C_0}{\pi}\exp\left(\frac{2k}{\pi\dot{a}}\right)\int_0^\infty \frac{\exp[-(1+\rho)\dot{a}\xi/D_\mathrm{a}]}{(1+\rho)\sqrt{\rho}}\left(\frac{\sqrt{1+\rho}+\sqrt{\rho}}{\sqrt{1+\rho}-\sqrt{\rho}}\right)^{\frac{k/\dot{a}}{\pi\sqrt{\rho(1+\rho)}}} \times\cos\left[\frac{k/\dot{a}-\rho(1+\rho)\dot{a}y/D_\mathrm{a}}{\sqrt{\rho(1+\rho)}}\right]\mathrm{d}\rho\,,\qquad \xi>0\,,\ y>0 \quad (23b)$$

Equation (23b) reveals that the concentration, and hence the interfacial flux $J_n=kC$, decrease exponentially ahead of the delamination tip in a narrow boundary layer of width on the order of $D_\mathrm{a}/\dot{a}$. The crack growth rate is (**?**)

$$\frac{\dot{a}}{k}=\sqrt{\frac{C_0 l}{2Q^*}} \tag{24}$$

and this value of $\dot{a}/k$ for $Q^*/(C_0 l)=0.01$ is plotted in Fig. 2(d). With this values of $\dot{a}/k$ inserted into (23b), the interfacial flux ahead of the delamination tip is obtained, and is included in Fig. 2(b). Very good agreement exists between the analytical and full numerical solutions.

3.4. Slow delamination growth

In order to derive approximate analytical solutions for regimes C and D, the quasi-steady problem of Section 3.2 is further specialised to the case $Q^*/(C_0 l)\gg 1$ such that $\dot{a}/k\ll 1$. Equation (16) then defines a regular perturbation problem such that the small parameter $\dot{a}/k$ multiplies a lower-order derivative. The leading-order solution to this problem is obtained by setting this small parameter to zero, such that (16) reduces to the Laplace equation

$$\frac{\partial^2 C}{\partial\xi^2}+\frac{\partial^2 C}{\partial y^2}=0 \tag{25}$$

Henceforth, the problem defined by (17), (21) and (25) is referred to as the *slow growth* problem. Note that the diffusion problem, as defined by

equation (25) and boundary conditions (17), does not depend explicitly on the growth rate $\dot{a}$. Its solution has the form

$$\frac{C}{C_0} = f_1\left(\frac{\xi}{l}, \frac{y}{l}; \frac{a}{l}, \frac{h_\mathrm{a}}{l}, \frac{K_\mathrm{d}}{lD_\mathrm{a}}\right) \tag{26}$$

and equation (21) is then used to determine the combined non-dimensional group $\dot{a}Q^*/(D_\mathrm{a}C_0)$, which can be used instead of the individual groups $\dot{a}/k$ and $Q^*/(C_0 l)$, such that (22b) reduces to

$$\frac{\dot{a}Q^*}{D_\mathrm{a}C_0} = f_2\left(\frac{a}{l}, \frac{h_\mathrm{a}}{l}, \frac{K_\mathrm{d}}{lD_\mathrm{a}}\right) \tag{27}$$

3.5. Regime C. Slow growth and bulk diffusion: K-field regime

Consider the case where growth is slow and bulk diffusion prevails, that is, regime C of Fig. 2(a). Fig. 2(b) shows that the interfacial flux presents an inverse square root singularity in the annular zone of approximate dimension $l \leq \xi \leq a$. In order to obtain an analytic expression for this singularity, consider the slow growth problem of Section 3.4. Take $K_\mathrm{d} = 0$, such that the boundary condition (17b) is replaced by $J_n = 0$ along $-a < \xi < 0$, $y = 0$; also, assume that $k \to \infty$ such that the boundary condition (17c) is replaced by $C = 0$ for $\xi > 0$, $y = 0$. The slow growth problem defined by the Laplace equation (25) and the foregoing boundary conditions can be solved in a circular region surrounding the delamination tip, by adopting polar coordinates (r, θ) centred on the delamination tip. The solution reads (**?**)

$$C(r,\theta) = \sqrt{\frac{2r}{\pi}}\frac{K}{D_\mathrm{a}}\sin\frac{\theta}{2} \tag{28a}$$

$$J_r(r,\theta) = -\frac{K}{\sqrt{2\pi r}}\sin\frac{\theta}{2} \tag{28b}$$

$$J_\theta(r,\theta) = -\frac{K}{\sqrt{2\pi r}}\cos\frac{\theta}{2} \tag{28c}$$

where $K = 2D_{\mathrm{a}}C_0/\sqrt{\pi a}$ for $a/h_{\mathrm{a}} \ll 1$. This solution is analogous to that for a Mode III crack in a linear elastic solid, where the out-of-plane displacement and shear stresses play the role of concentration and fluxes, respectively, the shear modulus plays the role of diffusion coefficient and K is termed the stress intensity factor (**?**).

For $l \leq \xi \leq a$, the interfacial flux is $J_n = -J_\theta(\xi, \theta = 0) = K/\sqrt{2\pi\xi}$. In contrast, for $0 < \xi \leq l$, the interfacial flux is approximately uniform and equal to the tip flux, see Fig. 2(b). The value of tip flux has been found in **?** by applying a K-field remotely from the delamination tip, and is given by $J_n = K/\sqrt{2l}$. For $\xi \geq a$, the interfacial flux is assumed to vanish. Thus the interfacial flux is given by:

$$J_n(\xi, y = 0) = \begin{cases} \dfrac{K}{\sqrt{2l}}\,, & 0 < \xi < \dfrac{l}{\pi} \\[2ex] \dfrac{K}{\sqrt{2\pi\xi}}\,, & \dfrac{l}{\pi} < \xi < \alpha a \\[2ex] 0\,, & \xi > \alpha a \end{cases} \tag{29}$$

where the parameter $\alpha = 1.3$ is calibrated from a best fit to the numerical results. Upon substituting (29) into the delamination criterion for slow growth, equation (21), the growth rate is

$$\frac{\dot{a}}{k} = \frac{C_0 l}{Q^*}\frac{\sqrt{2}}{\pi}\left(2\sqrt{\alpha} - \sqrt{\frac{l}{\pi a}}\right) \tag{30}$$

The growth rate $\dot{a}/k$ given by (30) for $Q^*/(C_0 l) = 10^4$ is plotted in Fig. 2(d) as a function of a/l. The analytic solution agrees very well with the numerical solution for $a/l > 1$. The interfacial flux distribution (29), plotted in Fig.

2(b), approximates very well the numerical solution. It is noted in passing that rearrangement of (30) gives

$$\frac{\dot{a}Q^*}{D_\mathrm{a}C_0} = \frac{\sqrt{2}}{\pi}\left(2\sqrt{\alpha} - \sqrt{\frac{l}{\pi a}}\right) \tag{31}$$

consistent with (27).

3.6. Regime D. Slow growth and surface diffusion: dislocation field regime

Now assume that slow growth occurs and surface diffusion dominates: case D of Fig. 2(a). Figure 2(b) shows that the interfacial flux is of the form of an inverse singularity in the annular domain $l \leq \xi \leq a$. Consider again the slow growth problem of Section 3.4, but now with $K_\mathrm{d} \to \infty$ such that the boundary condition (17b) is replaced by $C = C_0$ along $-a < \xi < 0$, $y = 0$. Also, take $k \to \infty$ such that $C = 0$ for $\xi > 0$, $y = 0$. The solution of the problem to the Laplace equation (25) and the above boundary conditions in a circular region surrounding the delamination tip is

$$C(\theta) = \frac{C_0\theta}{\pi} \tag{32a}$$

$$J_r = 0 \tag{32b}$$

$$J_\theta(r) = -\frac{D_\mathrm{a}C_0}{\pi r} \tag{32c}$$

This solution is the same as that for a screw dislocation in a linear elastic solid, where, again, the out-of-plane displacement and shear stresses play the role of concentration and fluxes, respectively, and the shear modulus plays the role of diffusion coefficient (**?**).

Now consider the more general case of a finite rate constant k, such that $l \equiv D_\mathrm{a}/k$ is also finite. The above analytical solution states that the interfacial

flux in the outer field is $J_n = -J_\theta(\xi) = D_\mathrm{a}C_0/(\pi\xi)$ for $l \leq \xi \leq a$. In contrast, for $0 < \xi \leq l$, the interfacial flux is almost uniform and is equal to the tip value such that $J_n = kC_0$. For $\xi \geq a$, it is assumed that the interfacial flux vanishes. Consequently, the distribution of interfacial flux is approximated by:

$$J_n(\xi, y=0) = \begin{cases} kC_0\,, & 0 < \xi < \dfrac{l}{\pi} \\ \dfrac{D_\mathrm{a}C_0}{\pi\xi}\,, & \dfrac{l}{\pi} < \xi < \beta a \\ 0\,, & \xi > \beta a \end{cases} \tag{33}$$

where the parameter $\beta = 2$ is obtained by calibration against numerical results. Finally, substitute (33) into (21) to obtain

$$\frac{\dot{a}}{k} = \frac{C_0 l}{Q^*}\frac{1}{\pi}\left[1 + \ln\left(\frac{\beta\pi a}{l}\right)\right] \tag{34}$$

The growth rate given by (34) for $Q^*/(C_0 l) = 10^4$ is plotted in Fig. 2(d) as a function of a/l. Excellent agreement with the numerical solution is observed for $a/l > 1$. The interfacial flux given by (33) is also in good agreement with the numerical flux, see Fig. 2(b). It is noted in passing that (34) can be re-expressed in the non-dimensional form as specified by (27).

Finally, note that analytical solutions for regimes B, C and D give the quasi-steady growth rate $\dot{a}(a)$ that is valid only after an initial transient of growth, see equations (24), (30) and (34). In principle, one could integrate such ODEs to obtain $a(t)$, but it would ignore the initial transient, as this would require the analytical expressions for $\dot{a}(a)$ to be valid throughout the entire growth history, and not just after an initial transient of growth. Therefore, analytical solutions for $a(t)$ have not been included in Fig. 2(c).

3.7. Slow growth and simultaneous bulk and surface diffusion

For the case of slow growth, the K-field regime and the dislocation field regime apply for $K_\mathrm{d} = 0$ and $K_\mathrm{d} \to \infty$, respectively, recall Sections 3.5 and 3.6. For intermediate values of K_d, the delamination growth rate can be estimated as a weighted average of the growth rates given by the K-field and the dislocation field solutions, equations (30) and (34), upon making use of a

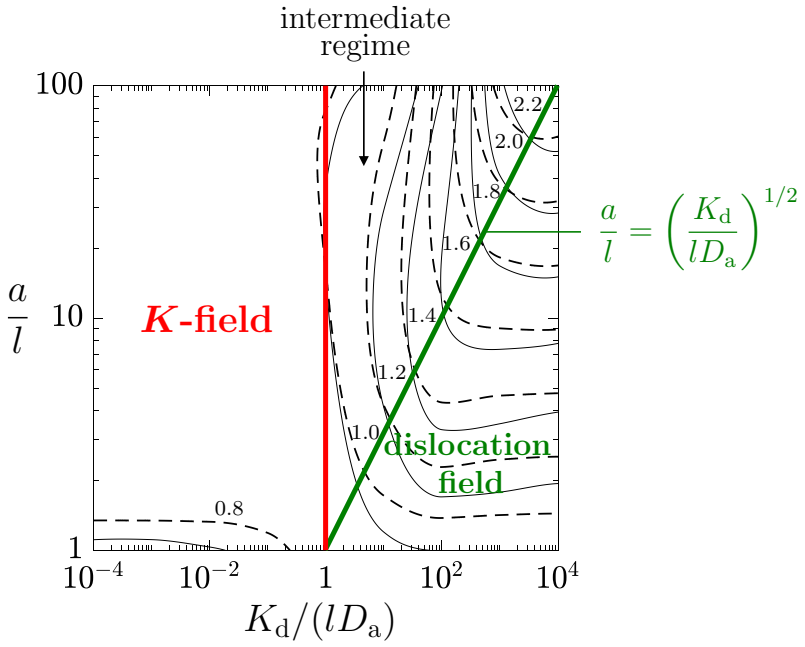

Figure 4: Contours of $\dot{a}Q^*/(D_\mathrm{a}C_0)$ on a plot of a/l versus $K_\mathrm{d}/(lD_\mathrm{a})$ for a thick sandwich layer and slow growth. The K-field and dislocation field regimes are identified on the map. Solid lines and dashed lines refer to the numerical solution of the full time-dependent problem (see Section 2) and to the analytic solution (35), respectively. The numerical solution is obtained for $a_0 = 0$, $h_\mathrm{a}/l = 1000$ and $Q^*/(C_0 l) = 10^4$.

weighting function w as follows:

$$\frac{\dot{a}Q^*}{D_\mathrm{a}C_0} = \frac{w}{\pi}\left[1+\ln\left(\frac{\beta\pi a}{l}\right)\right] + (1-w)\frac{\sqrt{2}}{\pi}\left(2\sqrt{\alpha}-\sqrt{\frac{l}{\pi a}}\right) \qquad (35)$$

where $w = 0$ for $K_\mathrm{d} = 0$ and $w = 1$ for $K_\mathrm{d} \to \infty$. A comparison with the numerical results suggests that an adequate expression for the weighting function is $w = K_\mathrm{d}/(K_\mathrm{d}+aD_\mathrm{a})$. Note that equation (35) has been conveniently written in terms of the combined group $\dot{a}Q^*/(D_\mathrm{a}C_0)$, in place of the single groups $\dot{a}/k$ and $Q^*/(C_0 l)$, to be consistent with (27).

Both numerical and analytical predictions of contours of $\dot{a}Q^*/(D_\mathrm{a}C_0)$ are plotted in Fig. 4 as a function of $K_\mathrm{d}/(lD_\mathrm{a})$ and a/l. The numerical solution is obtained by solving the full time-dependent problem of Section 2 for $a_0 = 0$, $h_\mathrm{a}/l = 1000$, $Q^*/(C_0 l) = 10^4$ and for selected values of $K_\mathrm{d}/(lD_\mathrm{a})$; contours are then obtained by interpolation. The regimes of validity of the K-field solution, equation (30), and dislocation field solution, equation (34), are indicated on the map: the K-field solution and the dislocation field solution are taken to be valid for $K_\mathrm{d}/(lD_\mathrm{a}) < 1$ and for $K_\mathrm{d}/(lD_\mathrm{a}) > (a/l)^2$, respectively.

4. Numerical solution and regimes of behaviour for a thin sandwich layer

The results presented in Fig. 2 refer to a thick sandwich layer, $h_\mathrm{a}/l = 1000$. In Fig. 5, the analysis of Fig. 2 is repeated for a thin sandwich layer of height $h_\mathrm{a}/l = 0.1$. Letters A', B', C' and D' denote the four representative regimes. A comparison with Fig. 2 reveals that the fast growth responses are very similar for the thick and the thin sandwich layers. In contrast, the slow growth response are different: the outer singularities in the interfacial

fluxes characterising the K-field and the dislocation field regimes for a thick sandwich layer (see Fig. 2(b)) are absent in a thin layer (see Fig. 5(b)), and new regimes of behaviour emerge instead. The regimes of behaviour for a thin sandwich layer are first summarised and then detailed.

Regime A': *Modified error function regime*

Bulk diffusion in the adhesive is dominant, $K_{\mathrm{d}}/(lD_{\mathrm{a}}) \ll 1$, and $Q^*/(C_0 l)$ is sufficiently small for delamination growth to be fast, $\dot{a}/k \gg 1$. The concentration profile is almost one-dimensional along x and is adequately described by a modified error function solution (**?**). The delamination length scales with the square root of time, and the solution is explained in more detail in Section 4.1.

Regime B': *Boundary layer regime*

Surface diffusion along the delamination is dominant, $K_{\mathrm{d}}/(lD_{\mathrm{a}}) \gg 1$, and $Q^*/(C_0 l)$ is again sufficiently small for delamination growth to be fast, $\dot{a}/k \gg 1$. A constant growth rate is established and the concentration decreases from C_0 to zero in a small boundary layer ahead of the delamination tip, as derived by **?**. This regime has already been discussed in Section 3.3, and is not repeated below.

Regime C': *Strip regime (bulk diffusion)*

Bulk diffusion in the adhesive is dominant, $K_{\mathrm{d}}/(lD_{\mathrm{a}}) \ll 1$, and $Q^*/(C_0 l)$ is sufficiently large for delamination growth to be slow, $\dot{a}/k \ll 1$. The concentration decreases exponentially ahead of the delamination tip and the growth rate is inversely proportional to the delamination length.

Regime D': *Strip regime (surface diffusion)*

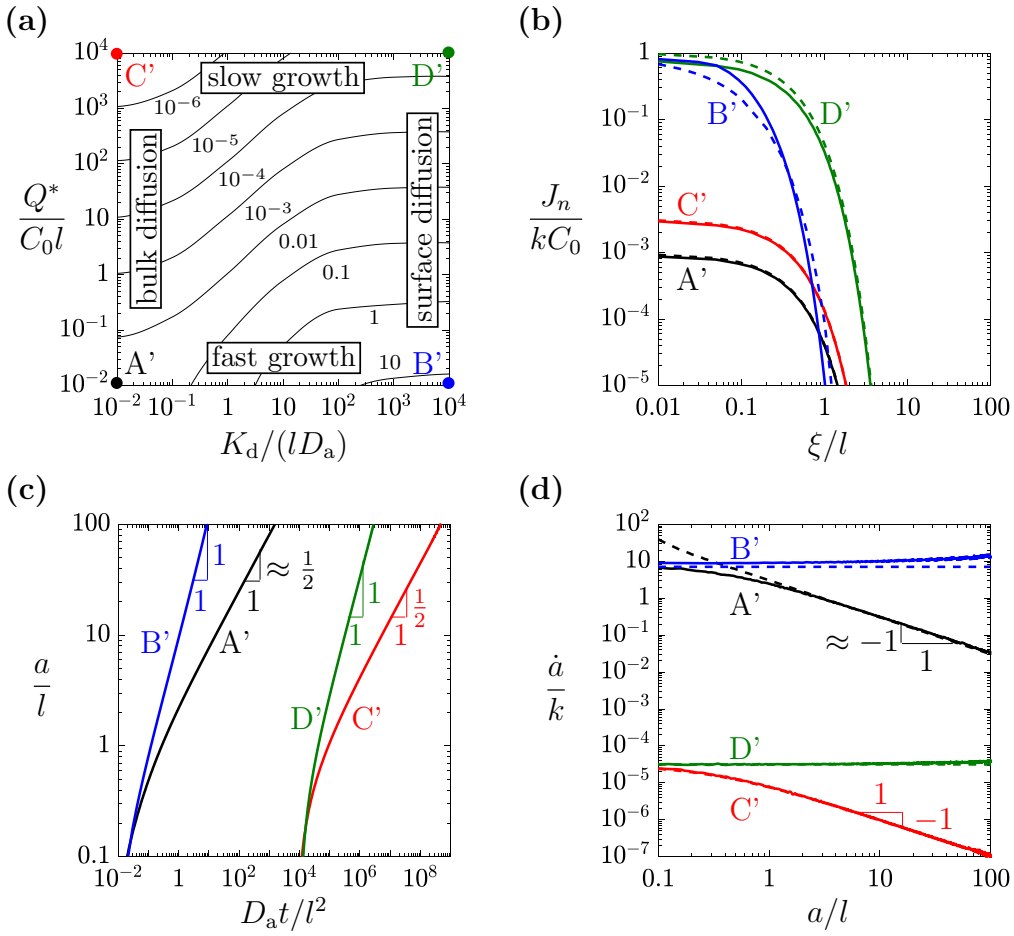

Figure 5: Numerical solution (solid lines) and analytical solution (dashed lines) for a thin sandwich layer, with $a_0 = 0$ and $h_\mathrm{a}/l = 0.1$. Regimes A', B', C' and D' and representative cases correspond to the modified error function, boundary layer, strip (bulk diffusion) and strip (surface diffusion) regimes, respectively. **(a)** contours of $\dot{a}/k$ on a plot with axes $K_\mathrm{d}/(lD_\mathrm{a})$ and $Q^*/(C_0 l)$ for the choice $a/l = 100$; **(b)** interfacial flux ahead of the delamination tip for $a/l = 100$; **(c)** delamination length as a function of time; **(d)** delamination velocity as a function of delamination length.

Surface diffusion along the delamination is dominant, $K_\mathrm{d}/(lD_\mathrm{a}) \gg 1$, and $Q^*/(C_0 l)$ is sufficiently large for delamination growth to be slow, $\dot{a}/k \ll 1$. The concentration decreases exponentially ahead of the delamination tip and the growth rate is constant.

The strip regime is presented in Section 4.2 for a finite value of K_d, and is then specialised to the two limiting cases of bulk diffusion ($K_\mathrm{d} = 0$) and surface diffusion ($K_\mathrm{d} \to \infty$).

4.1. Regime A'. Fast growth and bulk diffusion: modified error function regime

Consider the case of fast growth and bulk diffusion, that is, regime A' in Fig. 5(a). A 1D strip model is now introduced where the concentration in the adhesive is written as a function only of (x, t), independent of y. The governing equations are again (11). Notably, the sink term in equation (11b) cannot be neglected when l/h_a is large.

An approximate asymptotic solution for the concentration $C(\bar{x}, \bar{t})$ in the adhesive strip ahead of the delamination tip is found in terms of a small parameter $\varepsilon = h_\mathrm{a}/l \ll 1$. Then, (11b) becomes

$$\varepsilon \frac{\partial C}{\partial \bar{t}} = \varepsilon \frac{\partial^2 C}{\partial \bar{x}^2} - C \tag{36}$$

In the outer domain, that is, far from the delamination tip, ε can be set to zero in (36) such that $C = 0$. In order to find an inner solution valid close to the delamination tip, introduce the inner variable $\bar{\xi} = (\bar{x} - a/l)/\varepsilon$. Re-write (36) in terms of $\bar{\xi}$ to obtain

$$\varepsilon^2 \frac{\partial C}{\partial \bar{t}} = \frac{\partial^2 C}{\partial \bar{\xi}^2} - \varepsilon C \tag{37}$$

Neglect the second-order term in ε in (37) to obtain

$$C(\bar{\xi}, \bar{t}) = C_{\text{tip}}(\bar{t}) \exp\left(-\sqrt{\varepsilon}\bar{\xi}\right) \tag{38}$$

or equivalently, in dimensional form,

$$C(x, t) = C_{\text{tip}}(t) \exp\left(-\frac{x - a}{\lambda}\right) \tag{39}$$

with $\lambda = \sqrt{h_{\text{a}} l}$. Therefore, the concentration in the adhesive strip decays exponentially ahead of the delamination tip with decay length λ, starting from the time-dependent tip value $C_{\text{tip}}(t)$, which is unknown. The flux of corrodent along the adhesive layer is given by $J(x, t) = -D_{\text{a}}(\partial C/\partial x)$. Hence, the tip flux $J(a, t)$ is

$$J(a^+, t) = \frac{D_{\text{a}}}{\lambda} C_{\text{tip}}(t) \tag{40}$$

Behind the delamination tip, $x < a$, equation (10a) applies, with $C = C_0$ at $x = 0$. When a is large, the complementary error function solution (12) adequately approximates the concentration $C(x, t)$ in the adhesive layer for $x < a$. Consequently, the tip flux is also given by

$$J(a^-, t) = C_0 \sqrt{\frac{D_{\text{a}}}{\pi t}} \exp\left(-\frac{a^2}{4 D_{\text{a}} t}\right) \tag{41}$$

Now equate the two expressions for the tip flux as given by equations (40) and (41), to obtain

$$C_{\text{tip}}(t) = \frac{\lambda C_0}{\sqrt{\pi D_{\text{a}} t}} \exp\left(-\frac{a^2}{4 D_{\text{a}} t}\right) \tag{42}$$

Note that, except for the tip value C_{tip}, time does not enter the approximate solution for the concentration ahead of the delamination tip, see equation (39). Therefore, it is expected that the quasi-steady delamination criterion

(21) approximately holds. Upon combining equations (17c), (39) and (42), the reaction rate J_n ahead of the delamination tip is

$$J_n(\xi,t) = \frac{k\lambda C_0}{\sqrt{\pi D_{\rm a} t}} \exp\left(-\frac{a^2}{4D_{\rm a}t}\right) \exp\left(-\frac{\xi}{\lambda}\right) \tag{43}$$

where $\xi = x - a$. Finally, use (21) to obtain the delamination growth rate:

$$\dot{a} = \frac{k\lambda^2 C_0}{Q^*\sqrt{\pi D_{\rm a} t}} \exp\left(-\frac{a^2}{4D_{\rm a}t}\right) \tag{44}$$

This is an ODE in $a(t)$ which is solved numerically;[3] the numerical solution is then used to back-substitute for t as a function of a in (44). The resulting characteristic $\dot{a}(a)$ is plotted in Fig. 5(d). The reaction rate J_n as given by (43) is also plotted in Fig. 5(b). Excellent agreement with the numerical solution of the full time-dependent problem of Section 2 is observed for $a/l > 1$.

4.2. Regimes C' and D'. Slow growth: strip regime

Consider the slow growth problem of Section 3.4. If $h_{\rm a}/l \ll 1$, diffusion can be regarded as one-dimensional in the ξ direction, and the so-called strip regime is operative (**?**). Behind the delamination tip ($-a < \xi < 0$), a single homogenised strip of equivalent diffusivity $D_{\rm e}$ is considered such that $h_{\rm a}D_{\rm e} = K_{\rm d} + h_{\rm a}D_{\rm a}$, see Fig. 6(a). Mass conservation demands $\partial I_{\rm e}/\partial\xi = 0$, where $I_{\rm e} = -h_{\rm a}D_{\rm e}(\partial C/\partial\xi)$ is the corrodent current in the combined (homogenised) strip. Ahead of the delamination tip ($\xi > 0$), $\partial I_{\rm a}/\partial\xi = -kC$, where $I_{\rm a} = -h_{\rm a}D_{\rm a}(\partial C/\partial\xi)$ is the current in the adhesive layer. The above problem can be solved upon imposing the boundary conditions $C = C_0$ at $\xi = -a$ and $\lim_{\xi\to\infty} C = 0$, along with continuity of concentration and

[3] The *MATLAB* function *ode45* is used to obtain the numerical solution.

current at the delamination tip ($C|_{\xi=0^-} = C|_{\xi=0^+}$ and $I_\mathrm{e}|_{\xi=0^-} = I_\mathrm{a}|_{\xi=0^+}$). The concentration profile $C(\xi > 0)$ is (**?**):

$$C(\xi) = C_0 \left(1 + \frac{D_\mathrm{a}}{D_\mathrm{e}} \frac{a}{\lambda}\right)^{-1} \exp\left(-\frac{\xi}{\lambda}\right), \qquad \xi > 0 \tag{45}$$

where $\lambda = \sqrt{h_\mathrm{a} l}$. The flux follows immediately from the boundary condition (17c):

$$J_n(\xi) = kC_0 \left(1 + \frac{D_\mathrm{a}}{D_\mathrm{e}} \frac{a}{\lambda}\right)^{-1} \exp\left(-\frac{\xi}{\lambda}\right), \qquad \xi > 0 \tag{46}$$

Upon making use of (46), (21) gives

$$\frac{\dot{a}}{k} = \frac{C_0 \lambda}{Q^*} \left(1 + \frac{D_\mathrm{a}}{D_\mathrm{e}} \frac{a}{\lambda}\right)^{-1} \tag{47}$$

Now specialise equations (46) and (47) to the case C' of bulk diffusion ($K_\mathrm{d} = 0$, implying $D_\mathrm{e} = D_\mathrm{a}$) to obtain

$$J_n(\xi) = kC_0 \left(1 + \frac{a}{\lambda}\right)^{-1} \exp\left(-\frac{\xi}{\lambda}\right), \qquad \xi > 0 \tag{48a}$$

and

$$\frac{\dot{a}}{k} = \frac{C_0 \lambda}{Q^*} \left(1 + \frac{a}{\lambda}\right)^{-1} \tag{48b}$$

It follows immediately that, for $a/\lambda \gg 1$, the growth rate is inversely proportional to the delamination length. Equation (48a) is plotted in Fig. 5(b) for $h_\mathrm{a}/l = 0.1$ and $a/l = 100$, while equation (48b) is plotted in Fig. 5(d) for $h_\mathrm{a}/l = 0.1$ and $Q^*/(C_0 l) = 10^4$. Excellent agreement is evident with the full numerical solutions for the regime C'.

Alternatively, equations (46) and (47) can be specialised to the case D' of surface diffusion ($K_\mathrm{d} \to \infty$), such that

$$J_n(\xi) = kC_0 \exp\left(-\frac{\xi}{\lambda}\right), \qquad \xi > 0 \tag{49a}$$

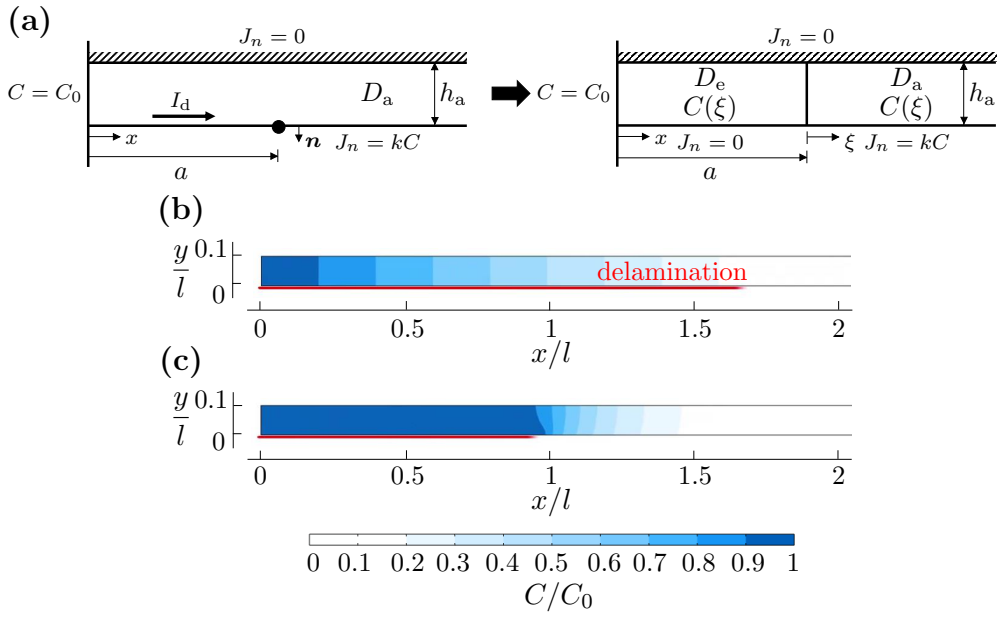

Figure 6: Slow growth in a thin sandwich layer: **(a)** the strip problem; concentration field in the sandwich layer and delamination length (denoted by a solid red line) at selected times, for the regimes **(b)** C' (strip regime, bulk diffusion) at $D_a t/l^2 = 2 \times 10^5$ and **(c)** D' (strip regime, surface diffusion) at $D_a t/l^2 = 4 \times 10^4$, as given by the numerical solution of the full time-dependent problem of Section 2 for $a_0 = 0$ and $h_a/l = 0.1$. Regimes C' and D' are identified in Fig. 5(a).

and

$$\frac{\dot{a}}{k} = \frac{C_0 \lambda}{Q^*} \tag{49b}$$

In contrast to case C' (equation (48b)), the growth rate is independent of delamination length. Equation (49a) is plotted in Fig. 5(b) for $h_a/l = 0.1$ and $a/l = 100$, while equation (49b) is plotted in Fig. 5(d) for $h_a/l = 0.1$ and $Q^*/(C_0 l) = 10^4$. Again, the analytic solutions are in excellent agreement with the full numerical solutions for the regime D'.

The concentration field in the adhesive domain and the associated delami-

nation length at selected times, as given by the full numerical solution, are given in Fig. 6(b) and (c) for the regimes C' and D' identified in Fig. 5(a). Full animations are included in the online Supplementary Material.

Finally, note that analytical solutions for cases A', C' and D' assume that a quasi-steady growth regime has been attained, see equations (44), (48b) and (49b). Therefore, as for Fig. 2, analytical solutions for $a(t)$ have not been included in Fig. 5(c).

5. Transition of response from thin to thick layer

It is worth investigating the range of values of h_a/l for which the different regimes of behaviour are operative. The combined group $\dot{a}/k$ is plotted in Fig. 7 as a function of h_a/l. The case of fast growth is considered in Fig. 7(a) by choosing $Q^*/(C_0 l) = 0.01$, whereas the case of slow growth is considered in Fig. 7(b) by taking $Q^*/(C_0 l) = 10^4$. In each plot a/l equals 100, and both numerical and analytical solutions are given.

In the case of fast growth and bulk diffusion (as denoted by A'-A in Fig. 7(a)), the error function solution (14) is accurate for $h_a/a > 1$, while the modified error function solution (44) is operative for $h_a/a < 1$. For fast growth and surface diffusion (B'-B in Fig. 7(a)), the boundary layer solution (24) is adequate in the full range of values of h_a/l considered. We note in passing that solution (24) assumes $a/l = h_a/l \to \infty$ and $\dot{a}/k \gg 1$ (**?**). Thus, exact alignment with the full numerical solution at finite $(a/l, h_a/l, \dot{a}/k)$ is not expected.

For the case of slow growth and bulk diffusion (C'-C in Fig. 7(b)), the K-field solution (30) is effective for $h_a/a > 1$, whereas the strip solution (48b)

is accurate for $h_a/a < 1$. In contrast, for slow growth and surface diffusion (D'-D in Fig. 7(b)), the dislocation field solution (34) holds for $h_a/a > 1$, whereas the strip solution (49b) is adequate for $h_a/l < 1$.

6. Effect of initial delamination length

So far, all solutions to the time-dependent growth problem of Section 2 have been reported for an initial delamination of vanishing length, $a_0 = 0$. The effect of a finite pre-existing delamination upon its subsequent growth is now reported.

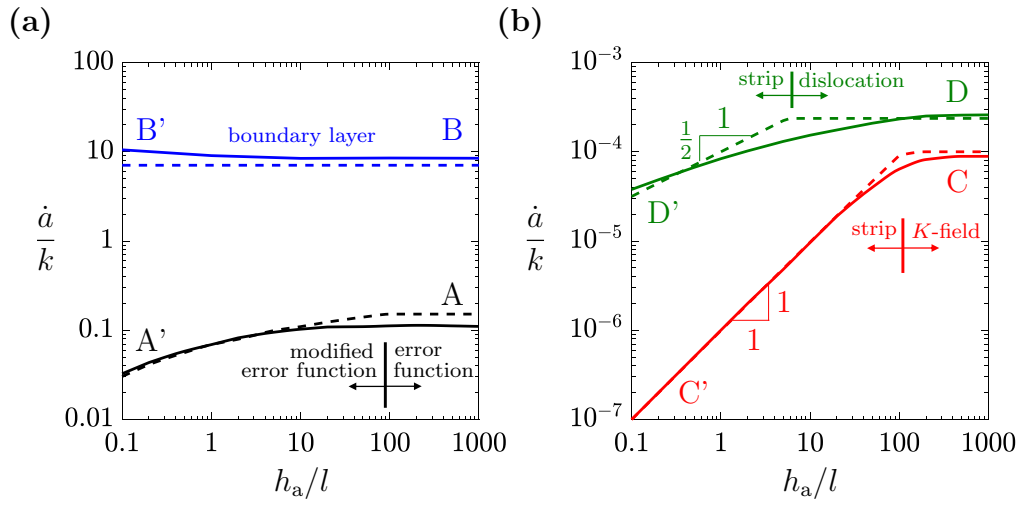

Figure 7: Non-dimensional growth rate, $\dot{a}Q^*/(D_a C_0)$, as a function of non-dimensional sandwich layer thickness, h_a/l, for $a/l = 100$ and for the cases of **(a)** fast growth and **(b)** slow growth. Solid lines and dashed lines refer to numerical solutions of the full time-dependent problem (see Section 2) and to analytic solutions (as given in Sections 3.1-3.6 and 4.1-4.2), respectively. Numerical solutions are obtained for $a_0 = 0$ and for either $Q^*/(C_0 l) = 0.01$ (fast growth) or $Q^*/(C_0 l) = 10^4$ (slow growth).

Consider the dependence of a/l upon $D_{\mathrm{a}}t/l^2$ for each representative case in regimes A-D, and $a_0/l = 0, 1$ and 10, see Fig. 8. After some initial growth, all curves for $a_0 > 0$ converge to the master curves for $a_0 = 0$. Consequently, the analytical estimates given above for the growth rate in the various regimes of behaviour are valid regardless of the value of a_0, provided that $a \gg a_0$.

When Q^* is sufficiently large (e.g., for regimes C and D in Fig. 8(c) and (d)), the initiation time for debonding t_{I} is approximated by $t_{\mathrm{I}} = Q^*/J_{\mathrm{tip}}$, where J_{tip} is the steady-state flux directly ahead of the tip of the pre-existing delamination (**?**). Then, after an initial transient of growth, a quasi-steady, slow growth rate is attained, as given in Sections 3.5, 3.6 or 4.2 depending on the operative regime of behaviour.

7. Concluding discussion

The growth of an interfacial delamination between a sandwich layer and its substrate has been analysed on the basis of the Fickian diffusion of a corrosive species from an external reservoir to the delamination tip, to feed an interfacial chemical reaction ahead of the delamination tip. The corrodent can diffuse both in the bulk adhesive and along the delamination. The delamination advances when a critical amount of corrodent has reacted directly ahead of the delamination tip.

When the critical amount of corrodent for debonding is large enough for the delamination velocity $\dot{a}$ to be much slower than the rate constant k of the reaction, a much simpler Laplace problem holds in a coordinate system that moves with the delamination tip. Then, the spatial integral of the reaction rate profile along the intact adhesive/metal interface can be used to estimate

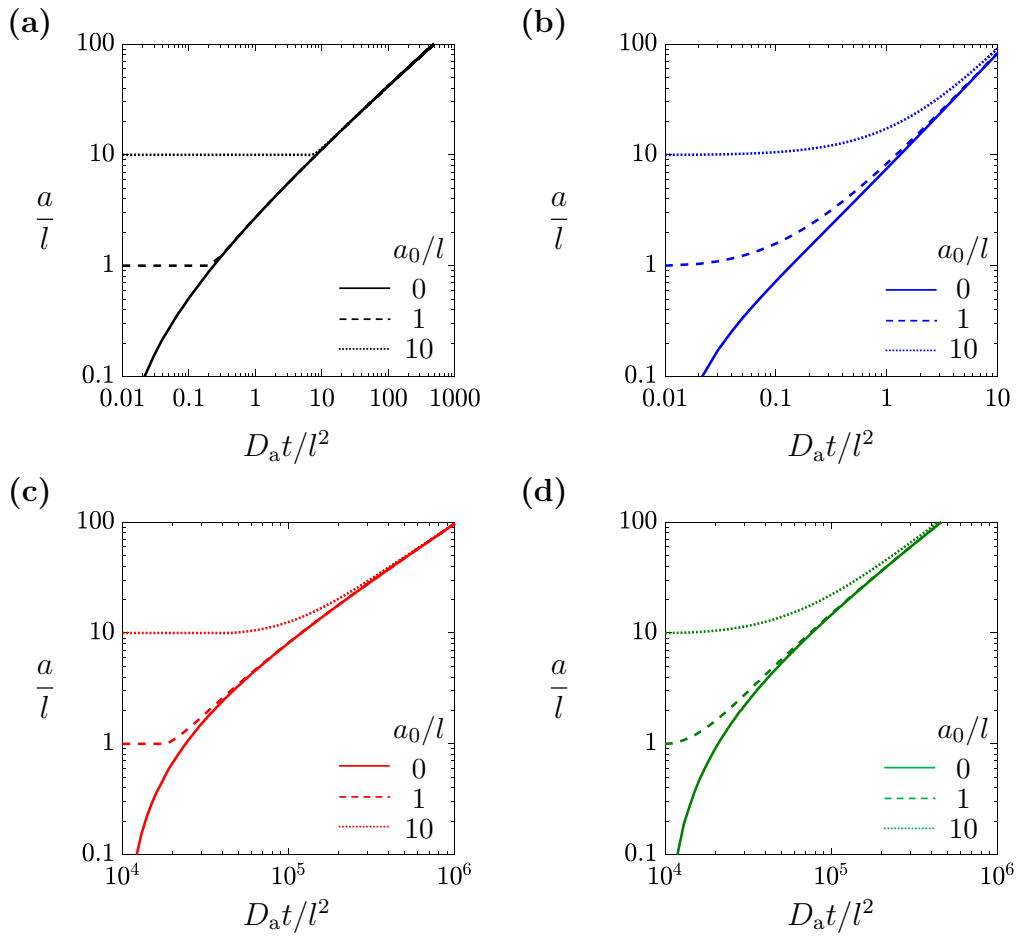

Figure 8: Effect of initial delamination length on delamination growth. Delamination length versus time for **(a)** regime A (error function regime), **(b)** regime B (boundary layer regime), **(c)** regime C (K-field regime) and **(d)** regime D (dislocation field regime). Regimes of behaviour are identified in Fig. 2.

the growth rate of the delamination. For a thick sandwich layer, the growth rate is governed by a singular field of flux that is reminiscent of a K-field in fracture mechanics or a dislocation field in elasticity theory. The nature of the singularity depends upon the relative magnitude of bulk to surface diffusion. Both singular fields are absent for a thin sandwich layer, and diffusion is essentially one-dimensional along a thin strip. The same regimes of behaviour were previously identified by **?** for the initiation problem.

The regions of approximate validity of the regimes of behaviour identified for a thick sandwich layer and for a thin sandwich layer are given in Figs. 9(a) and (b), respectively, for the choice $a/l = 100$. As evident from the comparison with numerical contours of $\dot{a}/k$, the analytical solution (35), valid for a thick layer and slow growth, gives an accurate estimate of the crack growth rate in the entire range of $K_{\rm d}/(lD_{\rm a})$ considered, and for a sufficiently large $Q^*/(C_0 l)$; the boundary layer solution (24) correctly captures the asymptotic crack growth rate for large $K_{\rm d}/(lD_{\rm a})$, provided that $Q^*/(C_0 l)$ is sufficiently small; the error function solution (13) is less accurate at predicting the asymptotic crack growth rate for small $K_{\rm d}/(lD_{\rm a})$, but still provides a reliable estimate, considering the very high sensitivity of $\dot{a}/k$ on $Q^*/C_0 l$ for this regime. In the case of a thin layer, the strip solution (47) is very accurate for any value of $K_{\rm d}/(lD_{\rm a})$ considered, and for a sufficiently large value of $Q^*/(C_0 l)$; the boundary layer solution (24) and modified error function solution (44) capture with good accuracy the asymptotic growth rates for large and small $K_{\rm d}/(lD_{\rm a})$, respectively, and for small $Q^*/(C_0 l)$.

The novelty of this study is to consider the growth problem in contrast to the initiation problem of **?**. The boundary condition moves with the crack

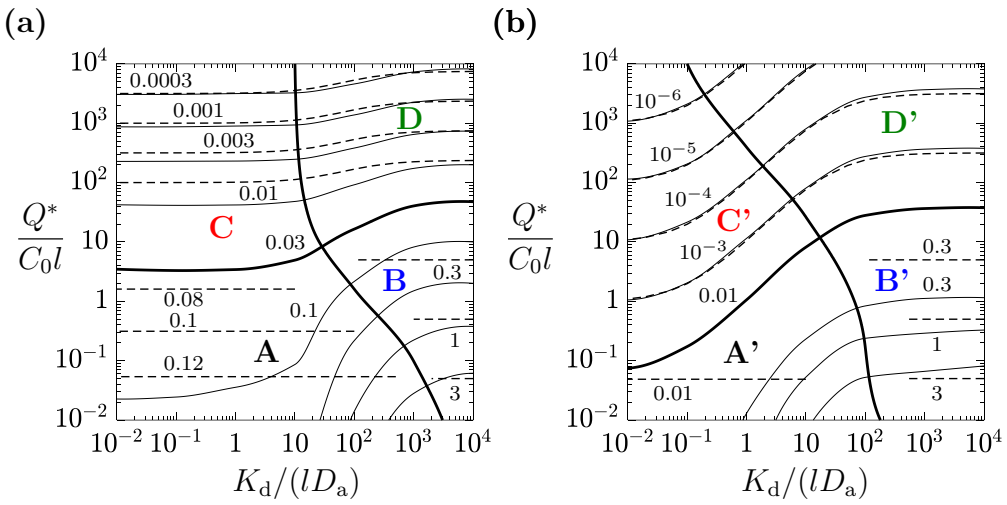

Figure 9: Contour map of $\dot{a}/k$ as a function of $K_\mathrm{d}/(lD_\mathrm{a})$ and $Q^*/(C_0 l)$, for $a/l = 100$ and **(a)** $h_\mathrm{a}/l = 1000$, **(b)** $h_\mathrm{a}/l = 0.1$. Solid lines denote numerical contours, whereas dashed lines denote analytical contours. Regimes of behaviour are indicated in the contour maps.

tip, and so the solution to the governing equations is different from that of the previous study. This situation is analogous to the problem of creep fracture: the solution for a growing crack is fundamentally different to that of a stationary crack (**?**). Attention is placed on the case of quasi-steady crack growth and the role of convected terms is analysed. The extent to which the solution for a stationary crack can be used to inform the solution for a growing crack is addressed. In particular, the regime of slow growth is identified for which the stationary crack solution applies.

Acknowledgements

The authors are grateful for financial support from the European Research Council in the form of an Advanced Grant (MULTILAT, 669764). The

authors are grateful to Prof. Vikram Deshpande and to Dr. Sina Askarinejad for insightful discussions.

Appendix A. Finite element implementation of the time-dependent growth problem

The solution of the time-dependent delamination growth problem illustrated in Section 2 is obtained via the commercial finite element software *COMSOL Multiphysics*, version 5.6. The `General Form PDE` interface is used to solve the PDE (3) with boundary conditions (1), (5) and (6). Linear Lagrange finite elements are used to approximate the unknown concentration field $C(x, y, t)$. In the implementation of the boundary condition (6), the active value of rate constant switches from value k to zero when the unknown variable $Q(x, t)$, defined in (7), attains the value Q^*. The boundary condition (5) is accounted for as a `Weak Contribution`.[4] Specifically, the diffusivity within the delamination switches from zero to the value D_{d} when $Q(x, t)$ attains the value Q^*. The above two expedients allow one to model the progressive advancement of the corrodent-filled delamination. The `Boundary ODEs and DAEs` interface within *COMSOL* is employed to solve for the unknown variable $Q(x, t)$. Specifically, the ODE $\partial Q/\partial t = J_n$, as given by (18), is solved for $Q(t)$ along the adhesive/metal interface, by employing quadratic discontinuous Lagrange finite elements. The discretised governing equations

[4] Implementing this boundary condition as a `Weak Contribution` allows one to reduce the derivation order in (5), and consequently to use linear polynomials to approximate the concentration field in the finite element formulation. It has been verified that the numerical solution does not change by increasing the order of the finite elements.

are solved for $C(x, y, t)$ and $Q(x, t)$ in a fully coupled manner in *COMSOL*.

A `Free Triangular` mesh is employed to discretise a finite computational domain of length $1000\,l$ in the x direction and variable height h_a in the y direction. The mesh is suitably refined in the proximity of the adhesive/metal interface. In particular, it is ensured that the elements adjacent to the adhesive/metal interface are always much smaller than l. For the choice $h_\mathrm{a}/l = 1000$, about 200 000 elements are used in the computational domain. The adhesive/substrate interface comprises 5 000 elements, whose size decreases in arithmetic sequence with x; the ratio between the largest and the smallest elements is equal to 50. Backward differentiation formulas are used for time integration. The time step is automatically chosen by the solver on the basis of the selected relative tolerance, which is set equal to 10^{-4}. Obtaining accurate numerical solutions for the case of surface diffusion, and fast growth especially, is challenging. It has been verified that the numerical solution obtained in *COMSOL* for this case is accurate by progressively decreasing the mesh size near the interface, and by specifying progressively stricter values for the relative tolerance in the time-dependent solver. The growth rate does not change further by decreasing the mesh size or the relative tolerance for time integration below the values reported above.